Bull. Chem. Soc. Ethiop. **2017**, 31(3), 383-396. ISSN 1011-3924

Printed in Ethiopia
DOI: http://dx.doi.org/10.4314/bcse.v31i3.3

# PHOTOCATALYTIC DEGRADATION OF CRYSTAL VIOLET BY THIOUREA-DOPED $TiO_2$ THIN FILM FIXED BED PHOTOREACTORS UNDER VISIBLE IRRADIATION: OPTIMISATION USING CENTRAL COMPOSITE DESIGNS AND KINETICS STUDIES BY MULTIVARIATE CURVE RESOLUTION

Hajar Khalilian[1*], Abolfazl Semnani[1] and Mohsen Nekoeinia[2]

[1]Department of chemistry, Faculty of Sciences, University of Shahrekord, Shahrekord, P.O. Box 115, Iran
[2]Department of chemistry, Payamnour University, Tehran, 19395-4697, Iran

(Received January 13, 2017; Revised December 17, 2017; Accepted December 21, 2017)

**ABSTRACT**. In this study, optimisation of the photocatalytic behaviour of crystal violet (CV) by thiourea (Tu)-codoped $TiO_2$ thin film in fixed bed photoreactor was investigated by central composite designs (CCDs). The effective variables were pH, the concentration of CV dye, flow rate and reaction time. The results of the CCD model showed a good agreement with experimental results, with $R^2 = 0.9680$ ($p < 0.0001$) and maximum degradation efficiency was obtained at the optimum conditions: dye concentration 8.5 mg/L, pH 9, flow rate 6 mL/min and reaction time 80 min. Subsequently, three absorbing chemical compounds presented in the degradation reaction were obtained by using singular value decomposition (SVD) method and evolving factor analysis (EFA). Then a multivariate curve resolution with alternating least squares (MCR-ALS) was performed to achieve the concentration and spectral profiles for each component. Finally, a hard modelling method was applied to determine the kinetic constants of distinct reactions occurred in the photocatalytic degradation process. The reaction rate constants were calculated for the first and second steps as $k_1 = 0.08327$ (SD = ±0.0015) /min and $k_2 = 0.045$ (SD = ±0.0006)/min, respectively.

**KEY WORDS**: $TiO_2$ thin film, Photocatalytic degradation, Central composite designs, Multivariate curve resolution, Kinetic studying

## INTRODUCTION

In recent years, removal of undesirable organic contaminants from water and wastewater is a major concern for the human communities. The organic contaminants are due to uncontrolled industrial wastewater, washout of agricultural lands which were polluted by pesticides or accidental leakage of tanks containing pollutants, etc.

Numerous studies have been carried out by researchers and scientists to find a complete and acceptable solution for this problem. A considerable number of these studies have been conducted by using $TiO_2$ photocatalytic oxidation method [1]. This method has been developed to degrade organic and inorganic pollutants into nontoxic species (e.g. $CO_2$, $H_2O$, etc.).

The use of $TiO_2$ nanoparticles has some limitations which are caused by the wide band gap between the valence and conduction bands ($Eg > 3.2$ eV, $\lambda < 388$ nm), that can only absorb UV light [2], so a modification of $TiO_2$ structure is necessary. One of the modifications is doping other atoms and ions (such as sulfur and nitrogen) to the titanium structure [3-8].

One of the important issues in photocatalytic system design is choosing between suspended or stabilized catalyst. In the case of suspended $TiO_2$ nanoparticles in contaminated water, it is necessary that these particles be recovered after treatment [9]. On the other hand, by using stabilized catalysts, there is no need for filtration.

In general, the development of $TiO_2$ thin film fixed bed photoreactors ensures more practical use of this process in large-scale deployments [10, 11].

*Corresponding author. E-mail: h.khalilian316@gmail.com

Several experimental design approaches such as the 3k factorial [12, 13], Doehlert [14], Box–Behnken and central composite designs (CCDs) [15-17] were applied to optimise the effective parameters in photoreactor systems. Also, chemometric methods such as SVD, EFA, and MCR-ALS [18, 19] were recommended to determine kinetic of organic molecules degradation [20].

In this work, CCDs were used to optimise and model the photocatalytic behaviour of CV by Tu-codoped$TiO_2$ thin film fixed bed photoreactor. The studied variables were pH, the concentration of CV dye, reaction time and flow rate. After obtaining the optimised values, SVD and EFA were used to obtain the number of chemical compounds presented in the reaction, then MCR-ALS [21-23] was performed to achieve the spectral and concentration profiles of each component. At last, a hard modelling method [24, 25] was applied to determine the kinetic constants of distinct reactions occurred in the photocatalytic degradation process.

## EXPERIMENTAL

### *Materials and reagents*

The reagents utilized in this work were analytical grade chemicals. CV dye ($\lambda_{max}$ = 590 nm) was obtained from Merck. Glass beads were used as support material (with 0.5 mm diameter).

### *Preparation of $TiO_2$ precursor sol*

$TiO_2$ was prepared by sol–gel as mentioned elsewhere [4]. Briefly, the sols were synthesized by adding acetylacetone (acac) ethanol and tetra butyl orthotitanate (TBOT) in acidic conditions at a ratio of 2.5:10:2.5 (acac : ethanol : TBOT). A clear and yellow solution was obtained by stirring with the magnetic force for 30 min. Then 2.0 mL of DI water was added to this solution and the specimen was magnetically stirred for 10 min. By adding concentrated HCl solution, the pH of the sol was adjusted at about 1.8, then 0.25 g thiourea (Tu) was added into prepared sol. Subsequently, the suspensions were stirred for about 2 h. Finally, the stable sol of the Tu-codoped $TiO_2$ was obtained and glass beads were covered with this sol by dip-coating and drying at 60 $^oC$ for 240 min; the beads were then heat-treated at 500 $^oC$ for 60 min.

### *Characterization techniques and software*

The surface morphology of the pure and Tu-codoped $TiO_2$ films was observed using scanning electron microscopy (SEM) (Philips XL-30ESM). Also, to distinguish the average crystalline size and crystal phase structure of $TiO_2$ nanoparticles powder, X-ray diffraction (XRD) measurements were performed by using a Philips X'pert Pro MPD model X-ray diffractometer using Cu $K\alpha$ radiation as the X-ray source in the 2θ range of 10–80$^o$.

Spectral data was observed using UV–Vis spectrophotometer (PG instruments Ltd). The UV–Visible spectra of the CV dye and blank specimen degradation were recorded at each nm from 250 to 700 nm, in which the blank solution only contained NaOH and $HClO_4$ (pH adjustment).

The design of experiments was carried out by "Design-Expert 7.0.0 Trial" (Stat-Ease Inc., Minneapolis) software. The recorded UV-Visible spectra were used to form the data matrices which were analysed by MCR-ALS in MATLAB 7 software environment.

### *Reactor*

The fixed bed photoreactor consisted of three glass tubes (7.5 mm i.d. and 200 mm length), these glass tubes were filled with $TiO_2$-coated glass beads and were positioned over a mirror. An HQI-BT 400W/D/DE40FLH1 Osram lamp was used to irradiate the fixed bed by visible light.

The distance between the glass tubes and the light source was 12 cm. All solutions were circulated into the reactor with a peristaltic pump at an adjustable flow rate (Agilent technology model BT100-1F).

*Experimental design and photocatalytic degradation procedure*

According to CCDs, the experimental conditions of each experiment were designed. A total of 30 photodegradation experiments and related responses (% degradation) are depicted in Table 1. The effective factors and their low and high levels were: 5-9 for the pH (A), 2-12 mL/min for flow rate (B), 1-13 $mg \cdot L^{-1}$ for the initial concentration of CV dye (C) and 20-100 min for reaction time (D).

All of the samples contained a 100 mL solution of CV dye or blank and pH was adjusted by adding diluted $HClO_4$ or NaOH. A fresh CV dye solution, with known concentration and adjusted pH, was poured into a reservoir with continuous stirring. The system was thermostated (Alpha Lauda model RA8) at 25 $^{o}$C for experimental design analysis. The CV dye solution was continuously circulated in the system by a peristaltic pump. The photocatalytic activities of immobilized $TiO_2$ were quantified using the degradation rate of CV dye and the following equation [26]:

$$Degradation(\%) = \frac{A_0 - A_t}{A_t} \tag{1}$$

where $A_0$ is the initial absorbance of the dye and $A_t$ is the absorbance of dye after the process. To find out the process noises, the degradation of blank solution ($H_2O$ + NaOH or $HCLO_4$) was attained under the same conditions of CV dye solution tests.

*Methodology and chemometric analysis*

Soft and hard MCR-ALS methods were utilized to obtain the chemical species concentration and spectral profiles and to estimate the rate constants of the photodegradation reactions. A detailed mathematical description of these techniques is mentioned in [27, 28]. However, these techniques are summarized in the two steps: (1) Obtaining data matrices at the optimum conditions from the UV–Visible spectra recorded during photodegradation of the CV dye ($D_d$ (i×j)) and blank ($D_b$ (i×j)), where i is the number of the recorded spectra (i = 22) and j is the number of the wavelengths (j = 451). (2) Using soft-modelling approach (MCR-ALS) which is based on the bilinear model according to the following relation:

$$D = C \times S^T + E \tag{2}$$

where C is the concentration profiles of each of the components present in the mixture, S contains the pure absorbance spectra of these components and E is the residuals or non-modelled absorbance data matrix. The following information could be obtained: (a) The number of chemical species is obtained by SVD and EFA from the augmented data matrixes. (b) The concentration and spectral profiles are estimated by the MCR-ALS and applied constraints, which includes a non-negativity constraint for both the concentration and spectral profiles and unimodality and closure constraints only for the concentration profile. (c) The rate constants according to CV dye degradation mechanism are calculated using mixed hard and soft MCR-ALS. For this purpose, after determining the number of chemical species and obtaining the profile of the concentrations by MCR-ALS, the rate laws of CV dye degradation reactions could

be composed regarding the components degradation mechanisms. The concentration profiles for any component in the reactions are set by a system of ODEs and then calculated by integration of these equations.

A time dependent matrix of concentration profiles is calculated for the species involved in the reaction, using the equations of the reactions for each component and an initial guess for the rate constants. Then the pure spectra of each presented component in the mixture is calculated by the following equation:

$$S^T = \left(C^T C\right)^{-1} C^T D \tag{3}$$

So the predicted response matrix is calculated as $\hat{D} = C \times S^T$ followed by calculating the sum-of-square of residuals:

$$ssq = \left\| \hat{D} - D \right\|^2 \tag{4}$$

The estimation of the rate constants was updated using nonlinear curve fitting technique to obtain the minimum value of ssq.

## RESULTS AND DISCUSSION

*Investigating the coated glass beads*

Figure 1 shows the (SEM) images of pure and Tu-codoped $TiO_2$ thin film. It is obvious that by adding Tu to the sol, the $TiO_2$ clearly lost its grain structure and transformed to the thin film. For the removal of free $TiO_2$ particles, the coated glass beads were fully washed with distilled water and used for other tests without losing their functionality.

The average crystalline size of the Tu-codoped $TiO_2$ film was calculated by Debye–Scherrer formula [29]. It can be seen from Figure 2 that the peaks in the XRD pattern are at $2\theta = 25.4^o$, $38.7^o$, and $48.1^o$, which represent the anatase form of $TiO_2$. Average crystal sizes of Tu-codoped $TiO_2$ were estimated to be 34–36 nm.

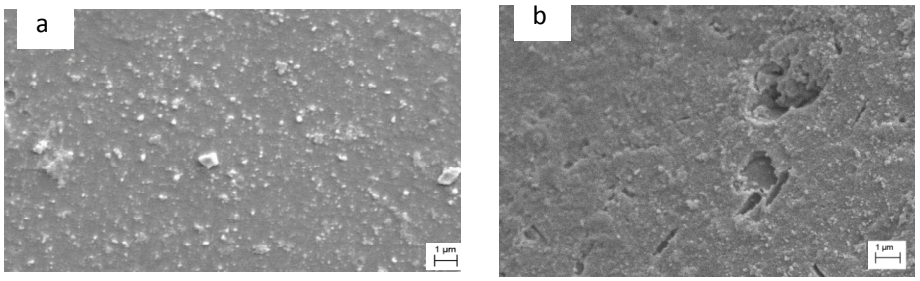


Figure 1. SEM image of $TiO_2$ thin films: (a) pure $TiO_2$, (b) Tu–$TiO_2$.

Table 1. CCD design matrix and observed %degradation for crystal violet in 30 different runs.

| Run | Block | A | B | C | D | % degradation |
|---|---|---|---|---|---|---|
| 1 | 1 | 8 | 4.5 | 4 | 40 | 77.39 |
| 2 | 1 | 8 | 9.5 | 4 | 80 | 93.74 |
| 3 | 1 | 6 | 4.5 | 4 | 80 | 91.91 |
| 4 | 1 | 7 | 7 | 7 | 60 | 80.72 |
| 5 | 1 | 6 | 9.5 | 4 | 40 | 81.16 |
| 6 | 1 | 7 | 7 | 7 | 60 | 86.60 |
| 7 | 1 | 8 | 9.5 | 10 | 40 | 63.46 |
| 8 | 1 | 6 | 4.5 | 10 | 40 | 51.40 |
| 9 | 1 | 6 | 9.5 | 10 | 80 | 79.52 |
| 10 | 1 | 8 | 4.5 | 10 | 80 | 90.65 |
| 11 | 2 | 7 | 7 | 7 | 60 | 85.92 |
| 12 | 2 | 6 | 4.5 | 4 | 40 | 78.64 |
| 13 | 2 | 6 | 9.5 | 4 | 80 | 96.99 |
| 14 | 2 | 8 | 9.5 | 10 | 80 | 88.16 |
| 15 | 2 | 6 | 4.5 | 10 | 80 | 86.93 |
| 16 | 2 | 7 | 7 | 7 | 60 | 90.04 |
| 17 | 2 | 8 | 4.5 | 4 | 80 | 95.62 |
| 18 | 2 | 6 | 9.5 | 10 | 40 | 41.89 |
| 19 | 2 | 8 | 4.5 | 10 | 40 | 66.65 |
| 20 | 2 | 8 | 9.5 | 4 | 40 | 92.91 |
| 21 | 3 | 7 | 12 | 7 | 60 | 85.38 |
| 22 | 3 | 7 | 7 | 7 | 100 | 96.38 |
| 23 | 3 | 7 | 7 | 7 | 20 | 52.21 |
| 24 | 3 | 9 | 7 | 7 | 60 | 87.90 |
| 25 | 3 | 5 | 7 | 7 | 60 | 85.75 |
| 26 | 3 | 7 | 7 | 7 | 60 | 88.23 |
| 27 | 3 | 7 | 7 | 13 | 60 | 52.77 |
| 28 | 3 | 7 | 7 | 7 | 60 | 89.32 |
| 29 | 3 | 7 | 2 | 7 | 60 | 82.34 |
| 30 | 3 | 7 | 7 | 1 | 60 | 100 |

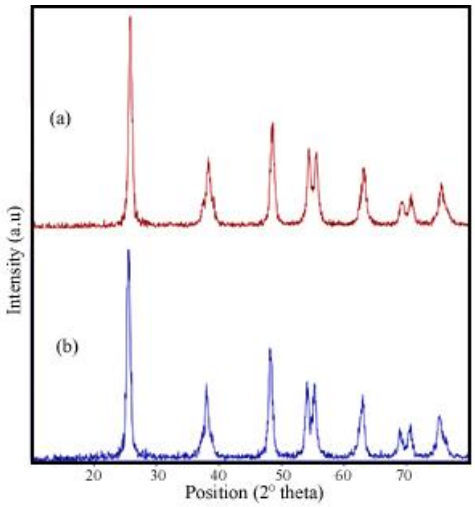


Figure 2. XRD pattern of $TiO_2$ powder (a) pure $TiO_2$ and (b) Tu–$TiO_2$.

*CCD model and residuals analysis*

The CCD design matrix and observed % degradation of CV dye are presented in Table 1. Where sufficient homogeneous experimental material is not available for all of the experimental runs, it becomes desirable to run them in blocks [30]. Three blocks are used in this study. A quadratic model was chosen from several models and was fitted to the results. After the analysis of variance (ANOVA), the regression equation was obtained, which represents the level of % degradation as a function of time, concentration, and pH. Table 2 shows the developed ANOVA model for % degradation of CV dye. In this table, p-value less than 0.050 (in confidence level 95%) shows that the effect of its corresponding factor is significant. The following equation gives a model that reasonably predicts the response variables in terms of significant factors.

$$Y = 26.7 + 1.7A - 6.69C + 1.825D - 0.2992C^2 - 0.00804D^2 + 0.432AB + 0.797AC - 0.1078AD - 0.365BC + 0.0768CD \quad (5)$$

In equation (5), A, B, C and D are pH, flow rate, the concentration of CV dye, and reaction time, respectively. It is obvious from equation (5) that in this model the main effects, interactions, and curvatures are considered. The ANOVA method has been used to calculate the model coefficients. Statistical parameters were obtained for this developed model. The coefficient of variation (CV, %) has a satisfactory value which is equal to 4.93. Also, the values of $R^2$, $R^2_{Adj}$ and $R^2_{Pred}$ are equal to 0.9680, 0.9336 and 0.7727, respectively. All of these statistical parameters in addition to the low value of prediction error sum of squares (PRESS) which equals 1485.9, confirmed the reliability of the proposed model.

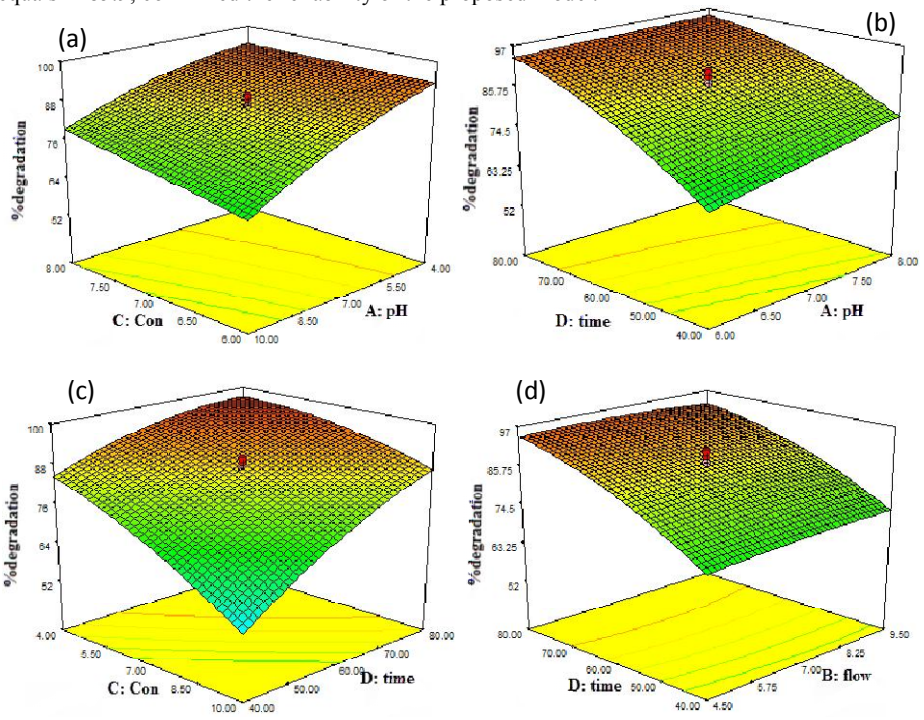


Figure 3. 3D response surface plots shows the change of % degradation as a function of following pair of factors, while the other factors maintaining constant at their central point values: (a) concentration of CV dye–pH, (b) time-pH, (c) time- concentration of CV dye and (d) time–flow rate.

By solving the system of equations of $\delta(Y)/\delta(A) = 0$, $\delta(Y)/\delta(C) = 0$, and $\delta(Y)/\delta(D) = 0$, the critical points of the response surface can be determined. In the ANOVA table, the value of flow rate (B) is not significant so its central point value (6 mL/min) has been chosen. The calculation method of response surface critical points has been published elsewhere [31]. The calculated values for the critical points are as follows: A = 9, C = 8.5 $mg \cdot L^{-1}$ and D = 80 min. In order to enhance our understanding of the effects of the independent variables and their interactions on the dependent variables, 3D response surface plots were plotted based on the model equation (Eq. (5)). Since the regression model has three independent variables, one variable was fixed to a constant at the central level for each plot. Figure 3 shows the 3D response surfaces as the functions of two variables at the centre level of other variables. Inspection of these figures shows that higher pH, lower concentration and higher time lead to a higher % degradation of CV dye. However, all of the significant factors (concentration, time and pH) should be considered simultaneously to obtain the optimum values.

Table 2. ANOVA statistical parameters for developed model.

| Source | Sum of squares | DOF* | Mean square | F-value | p-value | |
|---|---|---|---|---|---|---|
| Block | 43.88 | 2 | 21.94 | 1.37 | 0.290 | |
| Model | 452.11 | 14 | 6329.51 | 56.74 | < 0.0001 | Significant |
| A-pH | 173.07 | 1 | 173.07 | 10.77 | 0.0060 | |
| C- concentration | 2285.01 | 1 | 2285.01 | 142.19 | < 0.0001 | |
| D-time | 2781.51 | 1 | 2781.51 | 173.08 | < 0.0001 | |
| AC | 91.42 | 1 | 91.42 | 5.69 | 0.033 | |
| AD | 74.37 | 1 | 74.37 | 4.63 | 0.0509 | |
| BC | 120.09 | 1 | 120.09 | 7.47 | 0.0171 | |
| CD | 339.42 | 1 | 339.42 | 21.12 | 0.0005 | |
| $C^2$ | 198.83 | 1 | 198.83 | 12.37 | 0.0038 | |
| $D^2$ | 283.46 | 1 | 283.46 | 17.64 | 0.001 | |
| Residual | 208.92 | 13 | 16.07 | | | |
| Lack of Fit | 182.54 | 10 | 18.25 | 2.08 | 0.2977 | Not significant |
| Pure Error | 26.38 | 3 | 8.79 | | | |
| Corrected Total | 6582.31 | 29 | | | | |

* Degree of freedom (DOF)

*Analysis of photocatalytic degradation intermediates*

Figure 4 depicts the 3D visualization for the UV–Visible spectra which was achieved during the photodegradation process of CV dye in the optimum conditions. The intensity of the dye peaks is decreased during the degradation process, which shows the degradation of the dye into smaller detectable or undetectable molecular components. For determination of intermediate components, the SVD and EFA methods can be used.

For forming of D matrix, $D_1$, $D_2$ and $D_3$matrices were augmented as a column-wise matrix, $D = [D_1; D_2; D_3]$, in which $D_1$, $D_2$, and $D_3$ are data matrices that were obtained during the degradation of CV dye in optimum condition at T = 5 $^oC$, 15 $^oC$, and 25 $^oC$, respectively.

Table 3 shows the singular values achieved by SVD method for both the blank ($D_b$) and the dye ($D_d$) matrices. Since only one compound was presented in the process of the blank solution degradation, so the second singular value which was achieved from $D_b$ matrix. This singular value was selected to show the level of noise, which indicates three significant eigenvalues in $D_d$ matrix. These results revealed the presence of the intermediates in our photodegradation process [32].

Figure 5 shows the plot of EFA for the CV dye photodegradation process. The noise level is presented by a horizontal line which was acquired by EFA.

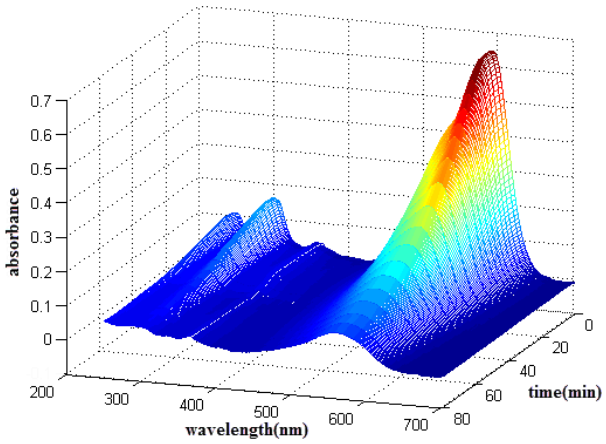


Figure 4. 3D visualization for the UV–Visible spectra obtained during the degradation of CV dye in optimum condition at T = 5 °C

Table 3. Singular values of $D_b$ and $D_d$ matrices. Only the first five values are shown.

| Factors | Blank | CV dye |
|---|---|---|
| 1 | 1.71402 | 27.0409 |
| 2 | 0.35950 | 3.16667 |
| 3 | 0.20806 | 0.76194 |
| 4 | 0.06904 | 0.23573 |
| 5 | 0.05390 | 0.17664 |

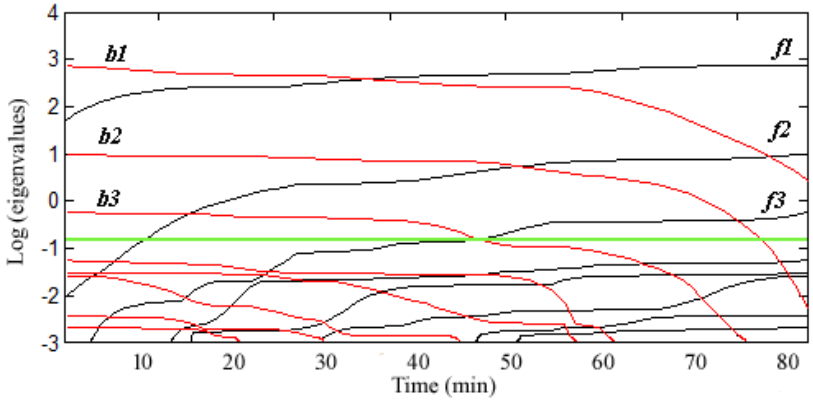


Figure 5. Results of the EFA for the spectral data matrix $D_d$. The horizontal line presents the noise level. Forward (f1, f2, and f3) and backward (b1, b2, and b3) directions.

It can be seen for the forward analysis, the variability is explained by one factor (f1) from the beginning of the process. Then at 7-12 min of reaction time, the second factor appears (f2), and the last factor becomes significant at 45-50 min (f3). It must be mentioned that the number

of effective factors which reflect the spectral evolution information is equal to the number of chemical components or equals the number of independent reactions +1 that is associated with the analysed spectra [33, 34]. Therefore, in this case, at 7-12 min the chemical variability is explained by one factor that is associated with the majority of untreated CV dye. After 7-12 min of reaction time, the second factor appears, showing another variability source that has become relevant. This can be related to the activation of another chemical component in the reactions process. After 45-50 min, the presence of another chemical component is indicated as a consequence of another reaction.

In the backward analysis, from 80 min to 75 min, there is only one factor (b1). From 75 to 40 min, two factors (b1 and b2) are the source of the variability and after 40 min of degradation process, the third one (b3) is observed.

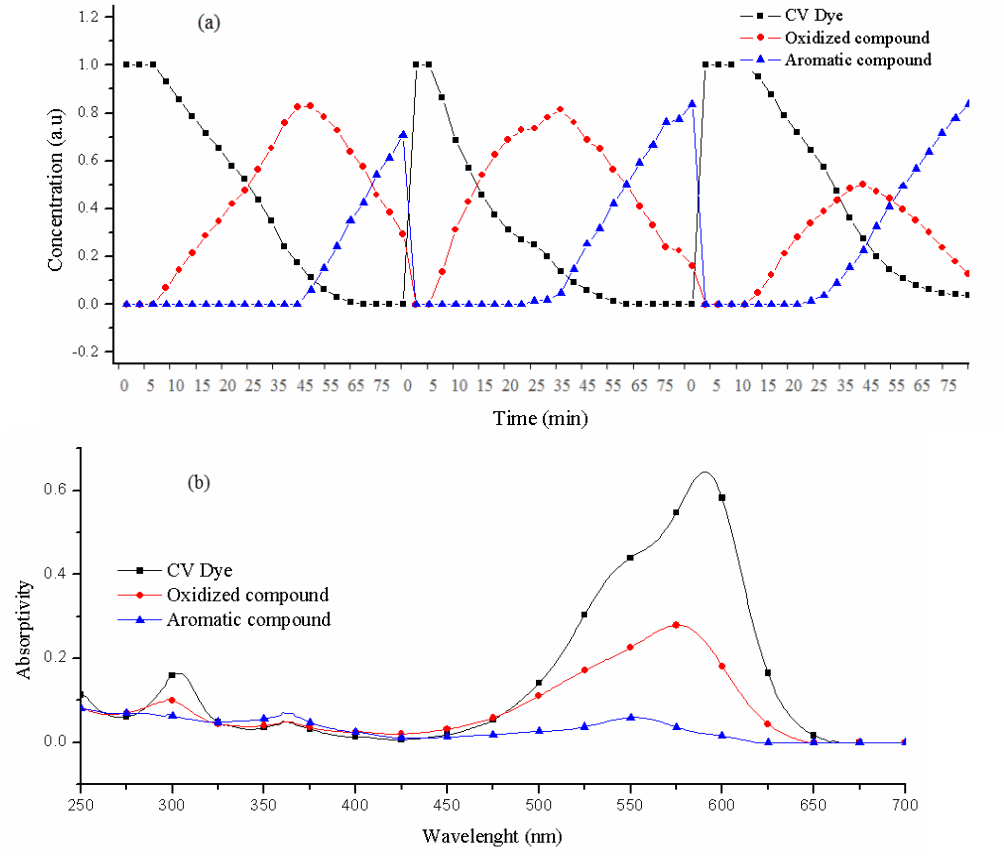


Figure 6. Concentration (a) and spectral (b) profiles of the chemical components involved in the photodegradation process retrieved by MCR-ALS.

Therefore, it could be assumed for $D_d$ that at least three components were actively involved in the UV-visible region. The MCR-ALS analysis can be used to retrieve information about these components for $D_d$ matrices. Figure 6 depicts optimal concentration (a) and spectral (b) profiles which show the behaviour of the chemical components affected in the degradation

process. The used parameters for evaluating the goodness of the optimisation process for matrix $D_d$ include LOF % PCA (7.225), LOF % EXP (7.352) and $R^2$ (99.469).

The spectral profiles (Figure 6b) are characterized by the initial CV dye (1) that absorbs in the visible region, also other components (2-3) which absorb at lower wavelengths. These profiles show the degradation of the CV dye and formation of the intermediates which are supposed to have a higher absorbance in the UV region with the smaller molecules sizes.

Figure 6a shows the concentration profiles during degradation process, which indicates that the initial CV dye (1) decreases with time, and it is near to zero at 55 min. After 5 min from reaction time, another component (2) is formed and increased until 20-35 min and then decreased during the process. After 20-45 min of the degradation process a new component (3) appears and is increased during the degradation process. This behaviour indicates that components 2 and 3 can be related to degradation intermediates and products, respectively. These results show a good agreement with the EFA plot of matrix $D_d$ (Figure 5). Also, this is supported by the parameters of goodness, which present a good agreement of the results.

*Determination of rate constants*

The complex molecular structure of CV dye leads to a difficult recognition of intermediates. Regardless of this drawback, taking into account the analysis of previous investigations [35-38], a reaction pathway for the degradation of CV dye could be proposed. The suggested reaction scheme is elaborated in Figure 7.

In the first step, the oxidized components were formed which involves N-demethylation of CV dye and cleavage chromosphere structure. This causes the loss of the aromatic conjugation and after the hydroxylation of intermediates, the hydroxylated species are oxidized to the quinoid compound. In the second step, aromatic rings were opened and carboxylic acids were produced, at the end, the opening rings undergo further degradation processes. The final degradation products could be $CO_2$ and $H_2O$. The latter situation is achieved only when the degradation process reaches the mineralization. The results of this section and those that were achieved by MCR-ALS are in a good accordance with each other (Figure 6).

Consideration of reaction pathways and degradation rates is critical for detection of waste water treatments and measuring their efficiency. The degradation rate constants of suggested reactions can be achieved by using hard and soft MCR-ALS modelling.

According to the mentioned results, the following kinetic model is proposed:

$$A \xrightarrow{k_1} B \quad (6a)$$

$$B \xrightarrow{k_2} C \quad (6b)$$

Here A, B, and C are associated with the CV dye, oxidized compound (N-demethylation of CV dye), a mixture of the aromatic compound and mineralization products in Figure 7. Also, according to the profiles of the degradation that were achieved by the MCR-ALS, the degradation rate of the intermediates and CV dye is higher than the formation rate of intermediates and final products.

The soft MCR-ALS concentration profiles were used to estimate the initial approximations of the rate constants, which were conformed to the pseudo-first-order kinetics as a common estimation in photodegradation processes [39-42]. So the following equation has been used:

$$\ln \frac{[CV\ dye]_0}{[CV\ dye]} = k_{ap} t \quad (7)$$

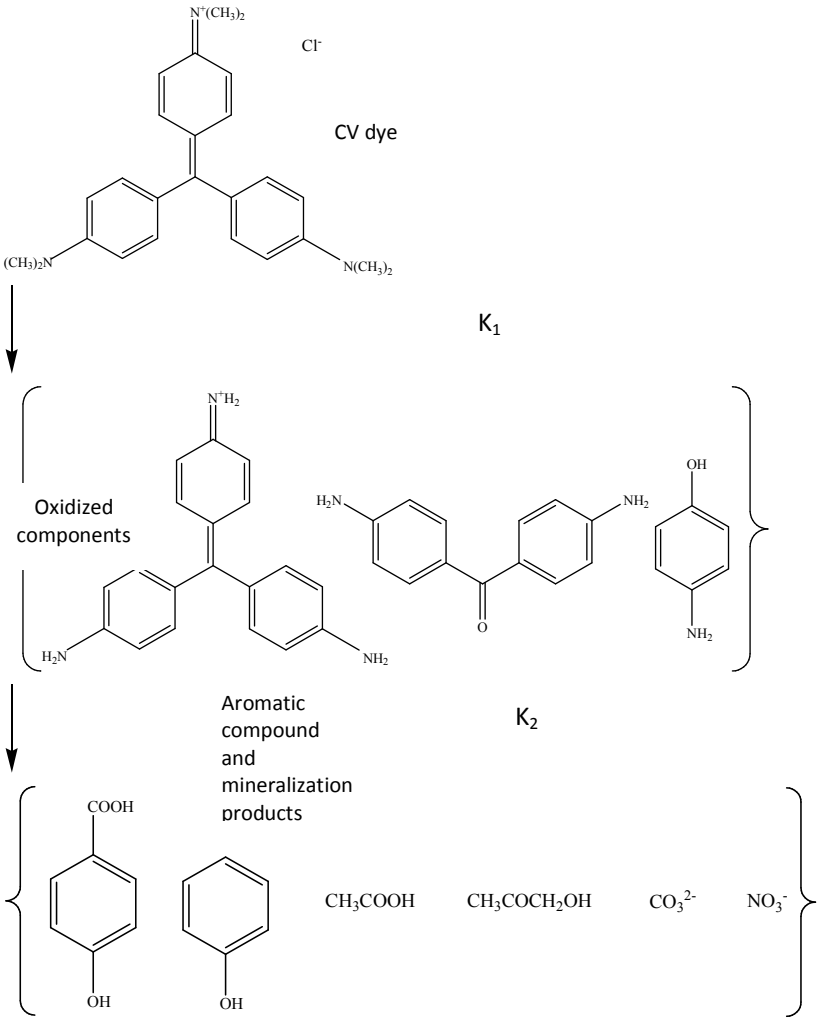


Figure 7. Proposed reaction pathway for CV dye photodegradation process.

The reaction equations applied in the mixed soft and hard MCR-ALS model were presented as follows:

$$\frac{\mathrm{d}}{\mathrm{d}t}A\left(t\right)=-k_1\cdot A\left(t\right); \tag{8a}$$

$$\frac{\mathrm{d}}{\mathrm{d}t}B\left(t\right)=k_1\cdot A\left(t\right)-k_2\cdot B\left(t\right); \tag{8b}$$

$$\frac{\mathrm{d}}{\mathrm{d}t}C\left(t\right)=k_2\cdot B\left(t\right); \tag{8c}$$

The dye spectra were retrieved by using hard and soft modelling and were compared with the experimental dye spectra, so the correlation factor of 99.96% was achieved. The kinetic constants values were: $k_1$ = 0.08327 (SD = ±0.0015) and $k_2$ = 0.045 (SD = ±0.0006). These results are in accordance with the soft MCR-ALS concentration profiles (Figure 6). After calculation of rate constants by using nonlinear curve fitting technique, the minimum ssq was achieved which is equal to 0.1510.

## CONCLUSIONS

The photocatalytic treatment of crystal violet in Tu-codoped $TiO_2$ thin film fixed bed photoreactor was optimised by CCDs. The optimum value of initial dye concentration, pH, flow rate and reaction time are 8.5 mg/L, 9, 6 mL/min, 80 min, respectively. The UV–visible spectra in optimum conditions were recorded during the degradation of CV dye. Then the collected spectra were treated by means of multivariate methods including mixed hard and soft MCR-ALS and EFA to determine the intermediates behaviour in the reactions.

The initial results of the components degradation and formation was obtained by EFA method, then based on this results, MCR-ALS determined the spectral and concentration profiles, and furthermore, the adequate information about the kinetic constants in the photodegradation process was achieved using mixed soft and hard MCR-ALS approach.

## ACKNOWLEDGMENTS

The authors would like to thank the Shahrekord University and Payamnour University for supporting this project. The authors also wish to thank Dr. Mehdi Moradi for his assistance in various stages of the work. This work was also partially supported by the Centre of Excellence for Mathematics, Shahrekord University.

## REFERENCES

1. Rodriguez, L.P.; Cuevas, S.M.; Oller, I.; Agüera, A.; Puma, G.L.; Malato, S. Treatment of emerging contaminants in wastewater treatment plants (WWTP) effluents by solar photocatalysis using low $TiO_2$ concentrations. *J. Hazard. Mater.* **2012**, 211-212, 131–137.
2. Lu, S.Y.; Wu, D.; Wang, Q.L.; Yan, J.; Buekens, A.G.; Cen, K.F. Photocatalytic decomposition on nano-$TiO_2$: Destruction of chloroaromatic compounds. *Chemosphere* **2011**, 82, 1215–1224.
3. Andersen, J.; Han, C.; O'Shea, K.; Dionysiou, D.D. Revealing the degradation intermediates and pathways of visible light-induced NF-$TiO_2$ photocatalysis of microcystin-LR. *Appl. Catal. B: Environ.* **2014**, 154–155, 259–266.
4. Behpour, M.; Atouf, V. Study of the photocatalytic activity of nanocrystalline S,N-codoped $TiO_2$ thin films and powders under visible and sun light irradiation. *Appl. Surf. Sci.* **2012**, 258, 6595– 6601.
5. Etacheri, V.; Seery, M.K.; Hinder, S.J.; Pillai, S.C. Nanostructured $Ti_{1-x}S_xO_{2-y}N_y$ heterojunctions for efficient visible-light-induced photocatalysis. *Inorg. Chem.* **2012**, 51, 7164–7173.
6. Hamadanian, M.; Reisi-Vanani, A.; Majedi, A. Preparation and characterization of S-doped $TiO_2$ nanoparticles, effect of calcination temperature and evaluation of photocatalytic activity. *Mater. Chem. Phys.* **2009**, 116, 376–382.
7. Rengifo-Herrera, J.A.; Pulgarin, C. Photocatalytic activity of N,S co-doped and N-doped commercial anatase $TiO_2$ powders towards phenol oxidation and *E. coli* inactivation under simulated solar light irradiation. *Solar Energy* **2010**, 84, 37–43.
8. Wang, J.; Li, H.; Li, H.; Zou, C. Mesoporous $TiO_{2-x}A_y$ (A = N, S) as a visible-light-response photocatalyst. *Solid. State. Sci.* **2010**, 12, 490–497.
9. Lee, J.H.; Nam, W.; Kang, M.; Han, G.Y.; Yoon, K.J.; Kim, M.S.; Ogino, K.; Miyata, S.; Choung, S.J. Design of two types of fluidized photo reactors and their photo-catalytic performances for degradation of methyl orange. *Appl. Catal. A: Gen.* **2003**, 244, 49–57.

10. García, N.M.; Suárez, S.; Sánchez, B.; Coronado, J.M.; Malato, S.; Maldonado, M.I. Photocatalytic degradation of emerging contaminants in municipal wastewater treatment plant effluents using immobilized $TiO_2$ in a solar pilot plant. *Appl. Catal. B: Environ.* **2011**, 103, 294–301.
11. García, N.M.; Maldonado, M.I.; Coronado, J.M.; Malato, S. Degradation study of 15 emerging contaminants at low concentration by immobilized $TiO_2$ in a pilot plant. *Catal. Today.* **2010**, 151, 107-113.
12. Sturini, M.; Rivagli, E.; Maraschi, F.; Speltini, A.; Profumo, A.; Albini, A. Photocatalytic reduction of vanadium(V) in $TiO_2$ suspension: Chemometric optimization and application to wastewaters. *J. Hazard. Mater.* **2013**, 254– 255, 179–184.
13. Schenone, A.V.; Conte, L.O.; Botta, M.A.; Alfano, O.M. Modeling and optimization of photo-Fenton degradation of 2,4-D using ferrioxalate complex and response surface methodology (RSM). *J. Environ. Manage.* **2015**, 155, 1-7.
14. Emilio, C.A.; Magallanes, J.F.; Litter, M.I. Chemometric study on the $TiO_2$-photocatalytic degradation of nitrilotriacetic acid. *Anal. Chim. Acta.* **2007**, 595, 89-97.
15. Khataee, A.R.; Kasiri, M.B.; Alidokht, L. Application of response surface methodology in the optimization of photocatalytic removal of environmental pollutants using nanocatalysts. *Environ. Technol.* **2011**, 32, 1669–1684.
16. Sleiman, M.; Vildozo, D.; Ferronato, C.; Chovelon, J.-M. Photocatalytic degradation of azo dye Metanil Yellow: Optimization and kinetic modeling using a chemometric approach. *Appl. Catal. B: Environ.* **2007**, 77, 1-11.
17. Khataee, A. R.; Fathinia, M.; Joo, S.W. Simultaneous monitoring of photocatalysis of three pharmaceuticals by immobilized $TiO_2$ nanoparticles: Chemometric assessment, intermediates identification and ecotoxicological evaluation. *Spectrochim. Acta A* **2013**, 112, 33-45.
18. Ni, Y.; Wang, S.; Kokot, S. Spectrometric study of the interaction between Alpinetin and bovine serum albumin using chemometrics approaches. *Anal. Chim. Acta.* **2010**, 663 139-146.
19. Kumar, K.; Mishra, A.K. Application of multivariate curve resolution alternating least square (MCR–ALS)'analysis to extract pure component synchronous fluorescence spectra at various wavelength offsets from total synchronous fluorescence spectroscopy (TSFS) data set of dilute aqueous solutions of fluorophores. *Chemometr. Intell. Lab.* **2012**, 116, 78-86.
20. Juan, A.D.; Maeder, M.; Martınez, M.; Tauler, R. Combining hard- and soft-modelling to solve kinetic problems. *Chemom. Intell. Lab. Syst.* **2000**, 54, 123–141.
21. Khataee, A.R.; Fathinia, M.; Naseri, A.; Hasanzadeh, A.; Vafaei, F.; Emami, A.; Hanifehpour, Y.; Joo, S.W. Modeling and optimization of simultaneous photocatalysis of three dyes on ceramic-coated $TiO_2$ nanoparticles using chemometrics methods: phytotoxicological assessment during degradation process. *Res. Chem. Intermed.* **2013**, 40, 1283-1302.
22. Kumar, K. Random initialisation of the spectral variables: an alternate approach for initiating multivariate curve resolution alternating least square (MCR-ALS) analysis. *J. Fluor.* **2017**, 27, 1957-1968.
23. Kumar, K.; Mishra, A.K. Multivariate curve resolution alternating least square (MCR-ALS) analysis on total synchronous fluorescence spectroscopy (TSFS) data sets: Comparing certain ways of arranging TSFS-based three-way array. *Chemometr. Intell. Lab.* **2015**, 147, 66-74.
24. Fernández, C.; Callao, M.P.; Larrechi, M.S. Kinetic analysis of C.I. Acid Yellow 9 photooxidative decolorization by UV–visible and chemometrics. *J. Hazard. Mater.* **2011**, 190, 986–992.
25. De Luca, M.; Ioele, G.; Mas, S.; Tauler, R.; Ragno, G.A study of pH-dependent photodegradation of amiloride by a multivariate curve resolution approach to combined kinetic and acid-base titration UV data. *Analyst.* **2012**, 137, 5428-35.

26. Eshaghi, A.; Mozaffarinia, R.; Pakshir, M.; Eshaghi, A. Photocatalytic properties of $TiO_2$ sol–gel modified nanocomposite film. *Ceram. Int.* **2011**, 37, 327–331.
27. Puxty, G.; Maeder, M.; Hungerbühler, K. Tutorial on the fitting of kinetics models to multivariate spectroscopic measurements with non-linear least-squares regression. *Chemometr. Intell. Lab.* **2006**, 81 149–164.
28. Maeder, M.; Neuhold, Y.M., *Practical Data Analysis in Chemistry*, Vol. 26, Elsevier: Netherlands; 2007.
29. Hamadanian, M.; Reisi-Vanani, A.; Majedi, A. Synthesis, characterization and effect of calcination temperature on phase transformation and photocatalytic activity of Cu,S-codoped $TiO_2$ nanoparticles. *Appl. Surf. Sci.* **2010**, 256, 1837–1844.
30. Box, G.E.; Behnken, D.W. Some new three level designs for the study of quantitative variables. *Technom.* **1960**, 2, 455-475.
31. Santos, W.L.d.; Santos, C.M.M.d.; Jorge L.O. Costa; Andrade, H.M.C.; Ferreira, S.L.C. Multivariate optimization and validation studies in on-line pre-concentration system for lead determination in drinking water and saline waste from oil refinery. *Microchem. J.* **2004**, 72, 123–129.
32. Aregahegn, Z.; Guesh, K.; Chandravanshi, B.S.; Pérez, E. Application of chemometric methods to resolve intermediates formed during photo-catalytic degradation of methyl orange and textile wastewater from Ethiopia. *Bull. Chem. Soc. Ethiop.* **2017**, 31, 223–232.
33. Ruckebusch, C.; Juan, A.D.; Duponchel, L.; Huvenne, J.P. Matrix augmentation for breaking rank-deficiency: A case study. *Chemometr. Intell. Lab.* **2006**, 80, 209–214.
34. Amrhein, M.; Srinivasan, B.; Bonvin, D.; Schumacher, M.M. On the rank deficiency and rank augmentation of the spectral measurement matrix. *Chemometr. Intell. Lab.* **1996**, 33, 17–33.
35. Fan, H.J.; Huang, S.T.; Chung, W.H.; Jan, J.L.; Lin, W.Y.; Chen, C.C. Degradation pathways of crystal violet by Fenton and Fenton-like systems: Condition optimization and intermediate separation and identificatio. *J. Hazard. Mater.* **2009**, 171, 1032–1044.
36. Couselo, N.; Einschlag, F.S.G.; Candal, R.J.; Jobbagy, M. Tungsten-doped $TiO_2$ vs pure $TiO_2$ photocatalysts: Effects on photobleaching kinetics and mechanism. *J. Phys. Chem. C* **2008**, 112, 1094–1100.
37. Li, X.; Liu, G.; Zhao, J. Two competitive primary processes in the photodegradation of cationic triarylmethane dyes under visible irradiation in $TiO_2$ dispersions. *New. J. Chem.* **1999**, 23, 1193–1196.
38. Ju, Y.; Fang, J.; Liu, X.; Xu, Z.; Ren, X.; Sun, C.; Yang, S.; Ren, Q.; Ding, Y.; Yu, K.; Wang, L.; Wei, Z. Photodegradation of crystal violet in $TiO_2$ suspensions using UV–Vis irradiation from two microwave-powered electrodeless discharge lamps (EDL-2): Products, mechanism and feasibility. *J. Hazard. Mater.* **2011**, 185, 1489–1498.
39. Xu, S.; Zhu, Y.; Jiang, L.; Dan, Y. Visible light induced photocatalytic degradation of methyl orange by polythiophene/$TiO_2$ composite particles. *Water Air Soil Pollut.* **2010**, 213, 151–159.
40. Behnajady, M.A.; Modirshahla, N.; Daneshvar, N.; Rabbanic, M. Photocatalytic degradation of an azo dye in a tubular continuous-flow photoreactor with immobilized $TiO_2$ on glass plates. *Chem. Eng. J.* **2007**, 127, 167–176.
41. Jiang, W.; Joens, J. A.; Dionysiou, D.D.; O'Shea, K.E. Optimization of photocatalytic performance of $TiO_2$ coated glass microspheres using response surface methodology and the application for degradation of dimethyl phthalate. *J. Photochem. Photobiol. A: Chem.* **2013**, 262, 7– 13.
42. Hosseini, S. N.; Borghei, S. M.; Vossoughi, M.; Taghavinia, N. Immobilization of $TiO_2$ on perlite granules for photocatalytic degradation of phenol. *Appl. Catal. B: Environ.* **2007**, 74(1), 53-62.